Journal for Electrochemistry and Plating Technology

JEPT

Edited by: DGO-Fachausschuss Forschung – Hilden / Germany

Square Wave Pulsating Overpotential Treatment of Chromic Acid Solution

Systematic investigation of square wave pulsating overpotential (SWPO) treatment of a chromic acid solution is presented. Some preliminary potentiodynamic scans, potentiostatic deposits, potential steps and capacitance vs. potential curves were measured in order to establish the practical range of the SWPO signal parameters. The results show that properly adjusting the electrochemical parameters of the cyclic alternating potential perturbation it is possible to obtain cracked or crack free metallic chromium or chromium oxide/hydroxide mixed coatings. The different deposit morphologies were characterized through scanning electron microscopy and their chemical composition and micro hardness was measured. Some insight into the possible mechanisms of coating growth under this potential cycling treatment is given.

Received: 2015-07-04
Received in revised form: 2015-XX-XX
Accepted: 2015-XX-XX

Keywords:
Chrome electroplating; Pulse electrolysis; Potentiodynamic Scans; Potential Steps

Author:
W. A. Egli

DOI:
10.12850/ISSN2196-0267.JEPT4937

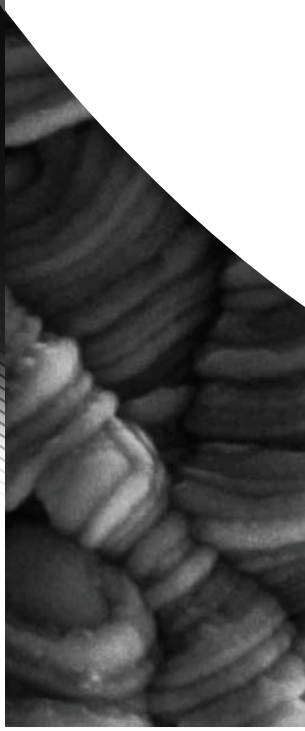

LEUZE VERLAG
seit 1902

Square Wave Pulsating Overpotential Treatment of Chromic Acid Solution

W. A. Egli

Independent Researcher of CICPBA., CIDEPINT – Av. 52 entre 121 y 122, (1900) La Plata, Argentina.
Email: anelpire3@cidepint.gov.ar, Phone: 0054/2227-15412879, FAX: 0054/2214-831141

Systematic investigation of square wave pulsating overpotential (SWPO) treatment of a chromic acid solution is presented. Some preliminary potentiodynamic scans, potentiostatic deposits, potential steps and capacitance vs. potential curves were measured in order to establish the practical range of the SWPO signal parameters. The results show that properly adjusting the electrochemical parameters of the cyclic alternating potential perturbation it is possible to obtain cracked or crack free metallic chromium or chromium oxide/hydroxide mixed coatings. The different deposit morphologies were characterized through scanning electron microscopy and their chemical composition and micro hardness was measured. Some insight into the possible mechanisms of coating growth under this potential cycling treatment is given.

Keywords: Chrome electroplating, Pulse electrolysis, Potentiodynamic Scans, Potential Steps
Paper: Received: 2015-04-21 / Received in revised form: 2015-XX-XX / Accepted: 2015-XX-XX
DOI: 10.12850/ISSN2196-0267.JEPT4937

1. Introduction

The electrodeposition of chrome from Cr^{+6} electrolytes has been one of the most widely used electroplating systems in the plating industry during the last decades. The usual direct current processes are based on chromic acid solutions with the addition of a catalyst, being sulfuric acid, fluoride compounds or a mix of them the most common ones [1-3]. The Sargent type electrolyte [4] is still being used in the plating industry in spite of the actual efforts to change to more friendly electrolytes based on Cr^{+3} formulations [2, 5-7]. The Cr^{+6} based electrolytes are mainly used for producing metallic chromium deposits of different hardness and brightness that fulfills a vast number of practical applications [2, 3, 8, 9]. Different chromium species, such as Cr_2O_3 and $Cr(OH)_3$, can be electrodeposited modifying bath formulations through the addition of nitrates, carbonates, fluorides or organic additives to the chromic acid solution. In that way it has been possible to obtain solar selective black chromium deposits on copper substrates for solar energy absorbing systems [10-13]. In last decades, the use of pulsed current and pulse reverse current techniques has been increasing because they improve coating quality and process performance [14-16]. In this work, systematic investigation of SWPO electrolysis of a CrO_3/H_2SO_4 electrolyte without levelling or brightening additives is presented. Preliminary cyclic voltammetry (CV), potentiostatic deposits (PD), potential steps and capacitance (C_E) vs. potential curves were done to characterize this rather complex electrochemical system and to establish the limiting values of the

parameters of the SWPO signal. The morphology and chemical composition of the electrodeposits was controlled selecting the SWPO perturbation parameters. It was possible to obtain classic cracked metallic chromium films, crack free chromium deposits, layers of faceted Cr_2O_3 crystals and leaf type morphologies of $Cr(OH)_3$. The oxidation number of chromium, the oxygen content and the hardness of the coatings varied markedly with the SWPO signal parameters. As a result of this investigation a new method to obtain chrome deposits with different chemical compositions and morphologies from the same Cr^{+6} electrolyte without additives has been developed. The resulting morphologies of the metallic chromium, chromium hydroxide and mixtures of chromium oxides are well characterized and some insight into the possible mechanism of coating growth is given.

2. Experimental

The electrolyte used was a conventional chrome plating bath containing 250 g L^{-1} CrO_3 and 2.5 g L^{-1} H_2SO_4 (S_{CR}). The working electrodes were 0.3 cm^2 surface area flat copper sheets cut from virgin circuit board plates, and the counter electrode was made of Pb-5%Sb alloy as is usually referred in the literature [2] with anode to cathode areas ratio of 20:1 [5] and the electrolyte volume was 100 ml. CV were done at a sweep rate of 20 mVs^{-1} at 50 ± 0.1ºC. PD were obtained on the copper cathodes under free convection at 50 ± 0.1ºC during 120 s. Short duration potential steps were applied to the copper cathodes in the plating electrolyte and 1 s current density (CD) transients were analyzed. C_E vs. potential curves were recorded for the copper electrodes in the chrome plating bath at 50 ± 0.1ºC considering a simple RC series equivalent circuit. A frequency of 1.5 kHz was chosen for the ac signal because the capacity readings were stable and reproducible in a frequency range from 0.5 to 3 kHz. A potential scan rate of 2 mVs^{-1} was applied and C_E was measured each 25 mV. The SWPO treatments were carried out cycling the electrode potential between an upper potential (E_U, during τ_u seconds) and a lower potential (E_L, during τ_l seconds) at 50 ± 0.1ºC in an open cell under potentiostatic control. A schematic of the SWPO function is shown in figure 1. The shape of the square wave was always symmetric ($\tau_u = \tau_l$) and the frequency (f) was fixed at 5 Hz ($\tau = 0.2$ s). In all the experiments the time of treatment was 10 minutes (3000 cycles).

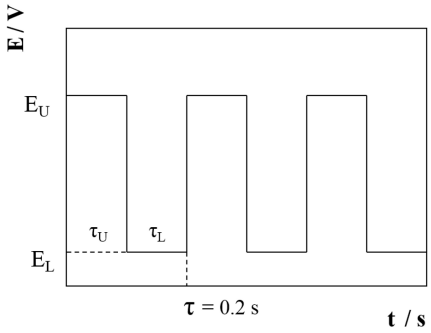

Fig. 1: Sketch showing a SWPO signal, alternating between E_L and E_U at a frequency $f = 1/(\tau_l+\tau_u)$

CV, PD and SWPO treatments were applied with a potentiostat-galvanostat Princeton Applied Research Mod. 273 with in-built signal generator and controlled by the SoftCorr 2 software. The ac electrochemical technique was applied with a frequency response analyzer Solartron 1255 connected with a potentiostat-galvanostat Solartron 1287 controlled with the Z-plot for Windows v 3.0 software.

In all the experiments a Cu-$CuSO_4$ (sat) reference electrode was used (Eº=0.316 V vs normal hydrogen electrode) and all the electrochemical potentials in this work are expressed in this

scale. SEM micrographs were recorded with a Quanta200 FEI equipment (Tungsten filament source). The composition of the coatings was evaluated using EDS. The detector scan mode with a step size of 0.05° and a sampling time of 3 s was used (scan rate 0.0167 º/s). X-ray photoemission spectroscopy (XPS) measurements were performed exciting with a radiation of 1253.6 eV (non-monochromatized X-ray Mg Ka source, 13 kV anode voltage and a power of 300 W). A two-point calibration of the energy scale was performed using sputtered gold and copper samples (Au 4f7/2 binding energy (BE) = 84.00 eV; Cu 2p3/2 BE = 932.67 eV). C 1s at 285 eV was used as charging reference. The hardness of each coating was determined averaging eight readings on its surface with a Shimadzu micro hardness tester with 15g loading during 5s.

3. Results

3.1 Cyclic voltammetry

In figure 2 it is shown the first CV cycle of a copper cathode in S_{CR} solution from 0.00 V to -1.20 V. During the forward scan two peaks were detected, marked as A and B. The cathodic processes occurring from -0.20 V to the CD minimum at -0.82 V

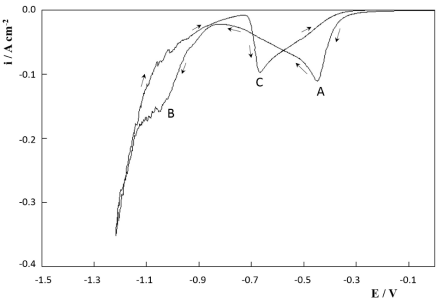

Fig. 2: First CV scan of a copper cathode in S_{CR} electrolyte at 20 mVs^{-1} and 50º C

are usually ascribed [17-21] to the formation of a Cr^{+3} oxide adsorbed film, formed by the reduction products of the reactions underlying peak A. R. Giovanardi et al [17] proposed an adsorption-desorption mechanism involving chromium species of different oxidation states partially covering the electrode surface:

Equation 1:

$$Cr_{sol}^{+6} + S + 2\,e^- \rightarrow Cr_{ads}^{+4}$$

Equation. 2:

$$Cr_{ads}^{+4} + e^- \rightarrow Cr_{ads}^{+3}$$

Equation 3:

$$Cr_{ads}^{+3} + e^- \rightarrow Cr_{ads}^{+2}$$

Where S stands for copper electrode free surface area with its characteristic surface density of electroactive sites. Cr_{sol}^{+6} is the concentration of Cr^{+6} in solution and Cr_{ads}^{+n} represent de chromium species adsorbed on the copper active sites (n=2, 3, 4). When the copper electrode potential is more cathodic than -0.82 V peak B start to grow, related to reaction (*3*) [17] and also to the start of bulk chromium deposition [19, 21]. H_2 evolution is negligible on copper cathodes but at sufficiently cathodic potentials it is combined with metallic chromium as unstable hydrides [22]. The decomposition of this hydrides during chrome plating are responsible of the cracking of the coating during electrodeposition [23].

The first backward scan in figure 2 shows one peak (C) at -0.74 V (E_C). CD is cathodic for forward and backward scans, indicating that the electrochemical reactions involved are irreversible [17, 24]. E_C was measured for switching potentials (SP) between -1.0 V and -1.3 V and the cathodic charge resulting from the integration of the area of peak C (Q_C) was calculated. As can be seen in figure 3,

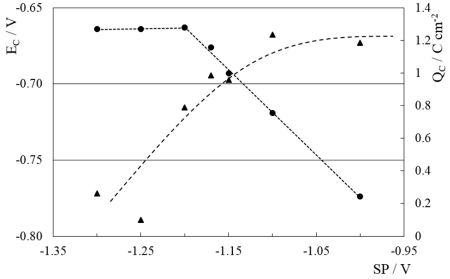

Fig. 3: Q_C (▲) and E_C (●) dependence with switching potential (SP)

E_C and Q_C both strongly depend on SP value. The shape of the backward scan on a metallic chromium surface in S_{CR} electrolyte is known to be a flat response [2, 3, 8, 9, 24]. For SP more cathodic than -1.25 V peak C practically disappears ($Q_C \approx 0$) indicating that the entire copper surface is covered with metallic chromium, thus inhibiting reactions *(1)*, *(2)* and *(3)* due to the absence of free S sites. This behavior indicates that the coverage of the Cu surface with metallic Cr increases with more cathodic SP values. It is important to remark here that for SP more anodic than - 0.80 V peak C does not show up, and this will be addressed again in section 3.3.

Other authors [25, 26] consider that peak A corresponds to Cr^{+6} to Cr^{+3} reduction and that its slight shoulder corresponds to incipient H^+ reduction, followed by a second passive region before the onset of Cr^{+6} to Crº reduction and H_2 evolution at peak B potentials. L. C. Jiang and D. Pletcher [24, 27] instead, postulated that peak B corresponds to Cr^{+3} to Crº reduction together with H_2 evolution. Survilene found that Cr^{+2} and hydrogen atoms are involved in the reaction mechanism [28]. There are some discrepancies between different investigators but most of them coincides on the formation of a thin layer very close to the electrode surface, made of Cr^{+6} reduction products, prior to bulk chromium deposition and that this process is responsible of peak A [29, 30]. The other common issue is that once this layer is formed, there is some evidence of passivation or at least a current reduction between peaks A and B [31, 32].

3.2 Potentiostatic deposits

PD were done on flat copper electrodes in S_{CR} electrolyte at selected potential values corresponding to some of the SP studied in 3.1. In figure 4 a) it is shown the SEM image of the electrode surface for E = -1.10 V. It was confirmed by EDS analysis that isolated chromium crystals of 2 µm average diameter size are obtained over the copper substrate. In figure 4 b) it is shown the SEM image of a deposit obtained at E= -1.20 V were an almost complete layer of chromium deposit is formed.

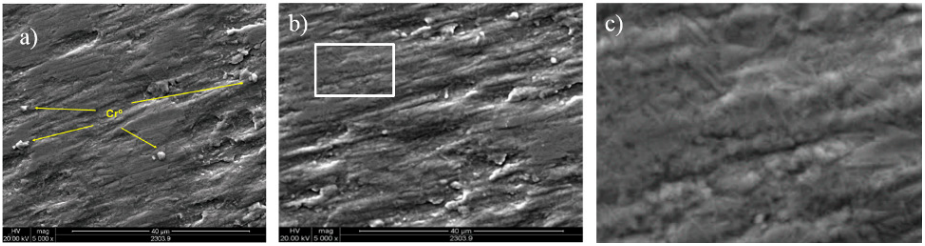

Fig. 4: SEM images of potentiostatic deposits on a copper cathode in S_{CR} electrolyte (50º C during 120 s) at a) -1.10 V, arrows indicate the isolated metallic chromium crystals, b) -1.20 V (5000X). c) zoom of rectangle in b) showing geometric details on the coating (15000X)

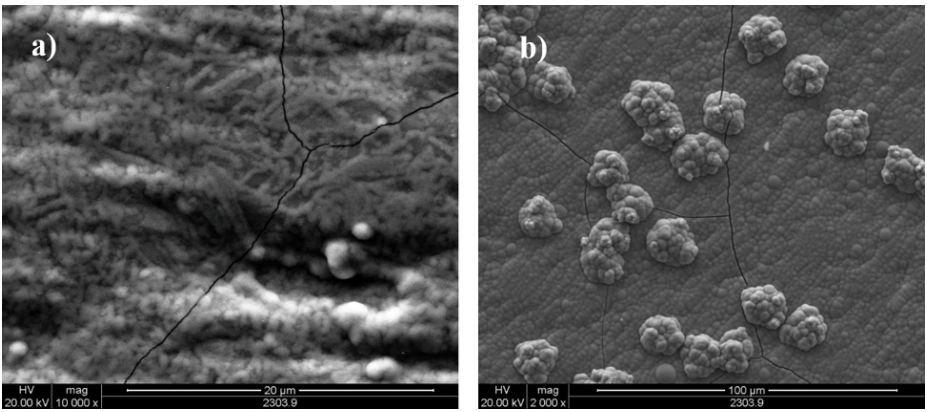

Fig. 5: SEM images of potentiostatic deposits on a copper cathode in S_{CR} electrolyte (50º C during 120 s) at a) -1.25 V (10000X), showing a network of crystals and the first cracks on the coating, b) SEM image representative of metallic chrome deposits for electrode potentials ≤ -1.35 V (2000X)

Very small geometric morphologies are observed at higher magnifications (figure 4 c)). The SEM image of figure 5 a) shows the coating obtained at E= -1.25 V, were the minimum of Q_C is observed (figure 3). In this case the very thin chromium layer is cracked and the entire electrode surface is covered by the metallic chromium deposit and a network of crystals is observed. The SEM pictures of the PDs are consistent with what was inferred from the CV analysis in 3.1. For PDs at more cathodic potentials (-1.25 V > E > -1.35 V) the classic cracked smooth chromium plated surface is obtained (not shown). At higher cathodic overpotentials (E ≤ -1.35 V) globular structures develop, like the "cauliflower" type described elsewhere [33] (figure 5 b)). It is clear from this picture that the cracks of the metallic coating are produced during the buildup of the film because some of the globular structures were grown over previously opened cracks and others are divided by the underlying fissures.

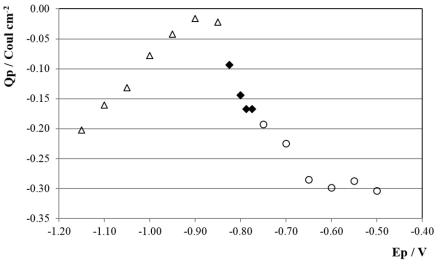

Fig. 6: Qp vs. Ep dependence for potential steps on copper cathodes in S_{CR} electrolyte at 50º C (○ diffusion, ♦ nucleation and growth and Δ flat transient behavior).

3.3 Potential steps

Copper cathodes were stabilized during 10 seconds at +0.50 V, then the potential was stepped to Ep and the CD transient was registered during 1 second. Ep was varied from -0.50 V to -1.15 V covering the potential zone between peaks A and B.

CD was integrated for each transient during 1 s and the charge density (Qp) was obtained for each Ep, showing the results in figure 6. For Ep between -0.50 and -0.75 V the transients show diffusion like behavior and the CD transients presented lineal i vs. $t^{-1/2}$ responses with i≈0 for t=0 (not shown), indicating that a diffusion process is involved and that the following relation holds:

Equation 4:

$i = n F D_o^{1/2} C^* / \pi^{1/2} t^{1/2}$

were all the variables and constants have their usual meaning. The slope was in average -0.14 ± 0.01. Considering $D_o \approx 1x10^{-5}$ cm^2s^{-1} and $C^* \approx 1/3\ C_{CrO3}$ because of polymerization of H_2CrO_4 [17, 34], we get from equation *(4)* an estimate of $n \approx 3$. This is consistent with Cr^{+6} to Cr^{+3} reduction previously described. For Ep between -0.78 and -0.83 V the CD transients show a characteristic nucleation and growth curve (figure 7).

This type of behavior has been assigned by Pletcher et al [24, 27] to the nucleation and growth of holes in a passive layer. This narrow potential range matches quite well with the electrochemical potential of the direct reduction of Cr_2O_3 to metallic chromium equilibria [35] (Equation *(15)* in section 4.2). If we consider pH≈-1 and make the temperature correction to 50°C [36] we get, from *(15)*, $E^{50} \approx -0.82$ V. This suggests that the nucleation and growth process could correspond to the reduction of the oxide layer and the birth of new metallic chromium nucleus, living "holes" in the previous passive layer. As was stated in 3.1 the fact that peak C does not appear for SP more anodic than -0.80 V is related with this phenomena. For Ep more cathodic than -0.83 V the CD transients show a flat response characteristic of the PD at short times (figure 7) and Qp is 95% smaller than for Ep ≤ -0,75 V, indicating that a new slow kinetic process starts. As it was shown in the previous section, this corresponds to the growth of the metallic chromium deposit. The direct Cr^{+6} reduction to bulk metallic chromium starts on the new born chromium phase, through the usually accepted mechanism [24, 25, 27, 31, 34], with the corresponding lower CD at this low cathodic overpotential for this reaction (3.2). When Ep reaches more cathodic values, Cr^{+6} reduction gets more important and CD and Qp grow again.

3.4 Capacitance vs. potential curves

Figure 8 shows the C_E vs. potential response for the copper cathodes in the S_{CR} solution at 50 ± 0.1 ºC. There is a very low C_E zone between +0.60 V and +0.15 V because of Cu passivation through the formation of an insoluble $CuCrO_4$ film. Near +0.10 V the corresponding Cu active to passive pseudo C_E maximum is observed. For E > +0.60 V transpasivity is reached.

From E = 0 V to -0.30 V a new C_E plateau is shown, with a minimum at ≈ -0.20 V indicating that this could be the potential of zero charge (pzc) of the cathode [37].

From -0.30 V to -0.78 V there is a new pseudo C_E loop corresponding to the diffusion transients described in 3.3. It is highly probable that this corresponds to

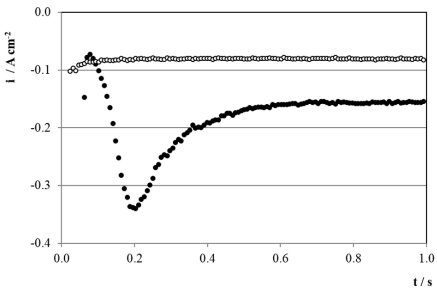

Fig. 7: Characteristic CD transients for Ep= -0.80 V (●) and Ep= -1.00 V (○)

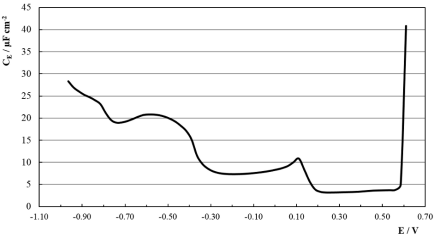

Fig. 8: C_E vs. potential curve for a copper cathode in S_{CR} electrolyte at 50º C and 1.5 kHz

the film formation described elsewhere [26, 29, 30, 34]. Although thermodynamically feasible, the reduction of Cr^{+6} to Cr^{+3} is kinetically inhibited until E = -0.30 V generating the pre-plating cathodic film which is widely accepted as high Cr^{+3} content. For - 0.83 V ≤ E ≤ - 0.78 V after another C_E arrest, a different process start, associated to the nucleation and growth depicted in 3.3. For E < - 0.83 V C_E continues to grow after a slight shoulder, probably related to reaction *(3)* [17, 28].

3.5 Square wave pulsating overpotential treatment

Based on the preceding results a relatively fast periodic SWPO was applied to the copper cathodes. E_L was fixed at -1.30 V, value sufficiently cathodic to obtain the reduced chromium species after peak A and B, but just before diffusion effects become important (3.2 and figure 5). Also from the curves of figure 3, at this E_L it is expected to obtain a complete coverage of the copper substrate. The E_U values were selected between -0.70 V and +0.50 V to vary the electrode potential through the different capacity plateaus in the anodic direction. Different types of deposits were obtained depending on E_U values.

For -0.70 V ≤ E_U < -0.40 V the deposits look very similar to the standard bright cracked metallic chromium coatings as in potentiostatic or galvanostatic electrolysis [2, 15]. In the case of setting -0,4 V ≤ E_U < -0,2 V the coatings morphology and their metallic luster is almost the same but cracks are absent. It is very interesting to remark that the cracks disappear when E_U is more anodic than E_A.

Moving to more anodic E_U values, a new type of deposit is obtained, shown in figure 9 a). In these cases the coatings are matt gray and their morphologies are facetted and exhibit a very peculiar structure that is maintained for -0.20 V ≤ E_U < +0.30 V, with slight changes in faceting. The average particle size is around 0.5 µm.

When E_U reaches +0.40 V and +0.50 V a new coating morphology appears, shown in figure 9 b). This type of coating, matt black, resembles the black coatings prepared with modified electrolytes reported elsewhere [12, 13].

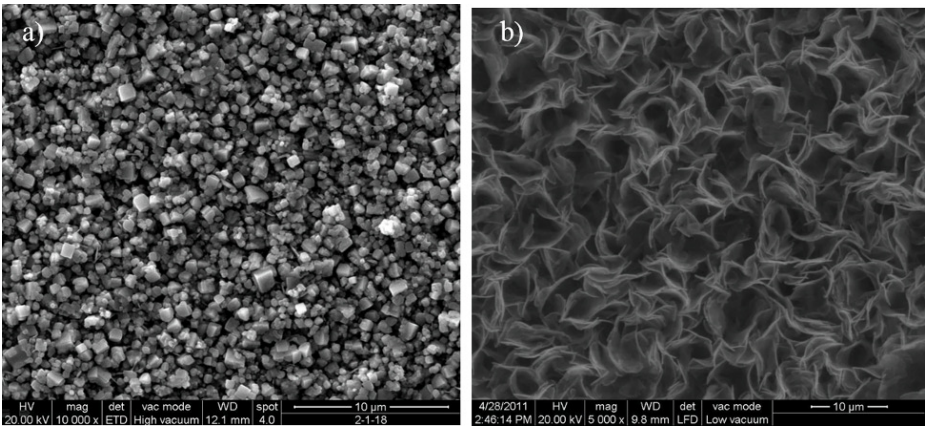

Fig. 9: SEM images of deposits obtained with SWPO treatment on the copper cathodes in S_{CR} electrolyte at a) E_U = -0.10 V and b) E_U = +0.50 V.

It is very interesting that for E_U just in the intermediate zone between the facetted type morphologies and the black coatings, an intermediate mixed coating is obtained (figure 10). In this case it is possible to distinguish both types of structures. This behavior is observed for E_U values between +0.30 V and +0.40 V. Finally for $E_U \geq +0.60$ V no Cr deposit is obtained.

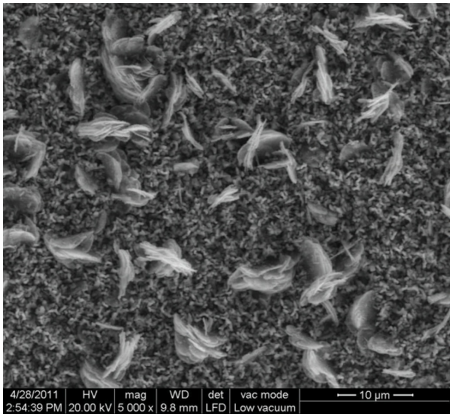

Fig. 10: SEM image of a deposit obtained with SWPO for E_U = +0.40 V.

3.6 Characterization of SWPO deposits

All the coatings obtained with the SWPO treatments were exhaustively washed with double distilled water, fast air dried and micro hardness and EDS quantitative analysis was done. The only elements detected where Cr and O. In figure 11 it is shown the dependence of the oxygen content in weight per cent ($O_{\%}$) with E_U. Based on the $O_{\%}$ values, it is possible to distinguish three zones: A) -0.70 V < E_U ≤ -0.20 V with $O_{\%}$ near to 10%; B) -0.20 V < E_U < +0.30 V with increasing $O_{\%}$ values almost reaching 30% and C) +0.30 V ≤ E_U ≤ +0.50 V, a very distinct zone where $O_{\%}$ start to grow with a sharp positive slope, reaching 50%. If we make an estimation of the $O_{\%}$ for Cr_2O_3 and for $Cr(OH)_3$ the approximate values are 30% and 50% correspondingly.

In order to correlate the $O_{\%}$ behavior with chemical composition of the coating some XPS determinations were done. It was concluded that in zone B the main chromium species were Cr_2O_3 and in zone C $Cr(OH)_3$. For the particular case of the coating obtained at E_U = +0.50 V the composition was 71% $Cr(OH)_3$ and 29% CrO_3. Accordingly for $E_U \geq +0.60$ V no deposit was obtained indicating that all the chromium species formed at E_L during τ_l are dissolved at E_U during τ_u.

The surface Vickers micro hardness of the SWPO coatings shown in figure 11 varies with E_U from the same value as the substrate at E_U = +0.50 V to three times this value at more cathodic E_U values. Here again the three different zones arises, A) with an average Hv between 200 and 300, B) with 150 constant value and a pronounced softening for C). The higher Hv values are found for E_U more cathodic than -0.20 V, that is when the coating is metallic Cr. The micro hardness was not measured in the cross section of the coatings due to the small thickness of the samples produced in this work (≈ 3 - 4 µm).

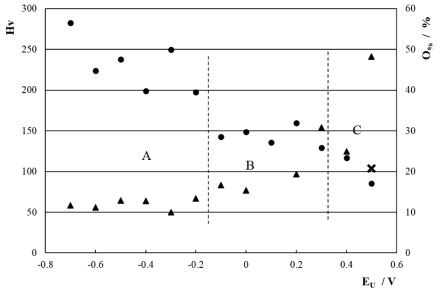

Fig. 11: Surface Vickers micro hardness (Hv; ●) and EDS oxygen content (O%; ▲) of SWPO deposits as a function of E_U. ✕ = Hv of substrate. Zones A, B and C are delimited with dashed lines.

4. Discussion

4.1 Current density transients during SWPO treatments

The average CD during application of E_U during τ_u;

Equation 5:

$$\langle i_u \rangle = 1/\tau_u \int_{n\tau_u}^{(n+1)\tau_u} i\,dt$$

was calculated for n=2000 (200 s), 4000 (400 s) and 6000 (600 s) for each SWPO treatment. The results are shown in figure 12. The dependence of $\langle i_u \rangle$ with E_U shows that for E_U more cathodic than -0.20V the CD is always cathodic and that $\langle i_u \rangle$ practically does not vary with time. This last behavior is probably related with the very smooth surface of the deposits obtained for these samples.

For E_U more anodic than -0.20 V, $\langle i_u \rangle > 0$, indicating that anodic processes prevails on the electrode during τ_u. It is also evident that $\langle i_u \rangle$ increases with time due to the surface roughening of the deposits during treatment (figures 9 and 10). Finally for E_U = -0.20 V, $\langle i_u \rangle = 0$, indicating that no net faradaic process occurs during τ_u and that it is invariant with time of treatment. The SEM images of figure 13 shows the morphology

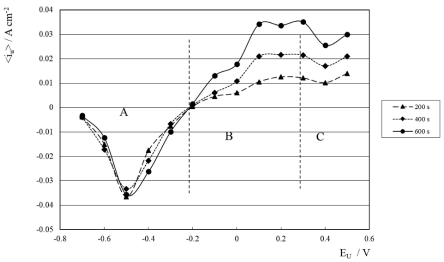

Fig. 12: Average CD $\langle i_u \rangle$ for 200, 400 and 600 s of SWPO treatment as a function of E_U. Zones A, B and C are delimited with dashed lines.

of this coating where it is possible to see a cubic structure with very well faceted crystals. It is interesting to remark that this point coincides with the possible pzc of the system as seen on C_E vs. E curve (figure 8). This E_U value is a transition point from which to more cathodic values the deposits are metallic chromium and to more anodic values the coatings are facetted structures with high oxygen content. As was observed on data of figure 11 we can differentiate zone A, B and C on $\langle i_u \rangle$ vs. E_U dependence on figure 12.

When we analyze the complementary average CD during the cathodic hemicycle of the SWPO treatment, $\langle i_l \rangle$, with integration limits in *(5)* from $(n+1)\,\tau_l$ to $(n+2)\,\tau_l$ for n = 2000, 4000 and 6000 at E_L = -1.30 V, we find that $(\langle i_l \rangle / \langle i_u \rangle)_{ti} \approx 10$. This is consistent with the asymmetric efficiencies of the deposition and dissolution processes in chrome plating [2, 5, 38]. Based on this, we can consider that practically all the reduced chromium species obtained at E_L during each τ_l, are electrochemically modified during next τ_u depending on E_U value. W. R. Rosas and A. Robin showed that for very short times the thin layer necessary to obtain metallic Cr during chrome plating is not formed [31], so during the SWPO treatment the formation of this type of deposit will depend on E_U. In that way, for E_U values more cathodic than -0.20 V (cathodic $\langle i_u \rangle$) it is possible to keep intact or even to build up the film during τ_u. As previously depicted in 3.5 the deposits obtained in this range of E_U values are all metallic chromium, with the lowest oxygen content. The fact that for E_U between -0.40 and -0.20 V the deposits are crack free is associated with the elimination of chromium hydride as in pulse reverse chrome plating [23].

For E_U values more anodic than -0.20 V the morphology and composition of deposits change abruptly and facetted crystallites are clearly seen.

It is also verified that for gradually more anodic E_U values the chromium oxides composition moves from Cr_2O_3 towards $Cr(OH)_3.nH_2O$. This was confirmed by EDS and XPS measurements. This evidence is also consistent with the oxygen content and the softening of the coatings (figure 11).

4.2 Thermodynamic considerations

From a thermodynamic point of view, the possible processes that can occur on the electrode during SWPO treatment, depending on the electrochemical potential and based on the chemical species found after the SWPO treatment are:

Equation 6:

$Cr^{+3} + 4H_2O = HCrO_4^- + 7H^+ + 3e^-$

$E_0 = 1.034 + 0.138\ pH + 0.0197\ \log(HCrO_4^-/Cr^{+3})$

Equation 7:

$Cr(OH)_3.nH_2O + H_2O = HCrO_4^- + 4H^+ + 3e^-$

$E_0 = 0.801 - 0.0788\ pH + 0.0197\ \log(HCrO_4^-)$

Equation 8:

$2Cr(OH)_3.nH_2O + H_2O = Cr_2O_7^{-2} + 8H^+ + nH_2O + 6e^-$

$E_0 = 0.785 - 0.0788\ pH + 0.0098\ \log(Cr_2O_7^{-2})$

Equation 9:

$Cr^{+2} + 4H_2O = HCrO_4^- + 7H^+ + 4e^-$

$E_0 = 0.311 + 0.1379\ pH + 0.0147\ \log(HCrO_4^-/Cr^{+2})$

Equation 10:

$Cr^{+2} + (3+n)H_2O = Cr(OH)_3.nH_2O + 3H^+ + e^-$

$E_0 = -0.027 - 0.1773\ pH - 0.0591\ \log(Cr^{+2})$

Equation 11:

$2\ Cr^{+2} + 3H_2O = Cr_2O_3 + 6H^+ + 2e^-$

$E_0 = -0.228 - 0.1773\ pH - 0.0591\ \log(Cr^{+2})$#

Equation 12:

$Cr + (3+n)H_2O = Cr(OH)_3.nH_2O + 3H^+ + 3e^-$

$E_0 = -0.676 - 0.0591\ pH$

Equation 13:

$Cr^{+2} = Cr^{+3} + e^-$

$E_0 = -0.723 + 0.0591\ \log(Cr^{+3}/\ Cr^{+2})$

Equation 14:

$2Cr + 3H_2O = Cr_2O_3 + 6H^+ + 6e^-$

$E_0 = -0.895 - 0.0591\ pH$

Equation 15:

$Cr = Cr^{+3} + 3e^-$

$E_0 = -1.060 + 0.0197\ \log(Cr^{+3})$

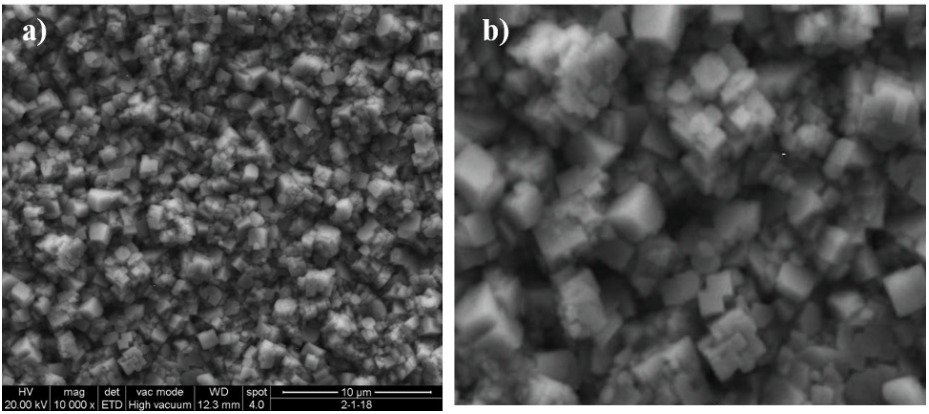

Fig. 13: SEM image of deposit obtained with SWPO treatment. E_U =-0.20 V. a) 10000X; b) 25000X.

Equation 16:

$Cr = Cr^{+2} + 2e^-$

$E_0 = -1.229 + 0.0295 \log(Cr^{+2})$

Based on the results obtained in 3.1 it is evident that some of these reactions are strongly inhibited on the Cu electrode (e.g. *6-8*). During the cathodic hemicycle of the SWPO, species like Cr^{+3}, Cr^{+2} and Crº will be formed on the electrode surface. The possible mechanisms could be quite complex and will be the result of a mix of some of the processes listed above. But considering the experimental evidence that for E_U more anodic than +0.60 V all these intermediate species are dissolved, suggests that Cr^{+2} could play a role on the processes occurring at E_L. This assertion can be postulated because the only equation that thermodynamically allows the direct oxidation of chromium species to a soluble compound at this potential value is *(9)*, after correcting the right potential value at 50º C. If we assume that the main active chromium species generated during τ_l is Cr^{+2} we can also understand through reactions *(10)* and *(11)* how the deposits depicted in 3.5 for E_U between -0.20 and +0.30 V could be grown. The continuous build up of the gray and black chromium oxides/hydroxides films described in 4.1 suggests that the Cr_2O_3 and $Cr(OH)_3.nH_2O$ are irreversibly formed on the cathode surface. That means that during each cycle of the SWPO signal Cr^{+2} is formed at E_L during τ_l, and then this Cr^{+2} is oxidized at E_U during next τ_u to the corresponding Cr^{+3} compound. As this is a dynamic model, not in equilibrium, the thermodynamic considerations has to be considered as feasibility limits.

For the metallic chromium deposits obtained for $-0.70\ V \leq E_U < -0.20\ V$ it is clear that during τ_u at this electrode potentials the pre plating layer necessary for obtaining metallic chromium is not destroyed. In that way the usually accepted chrome plating mechanism will be possible during both hemicycles of the SWPO treatment ($\tau_l + \tau_u$).

5.Conclusions

Based on preliminary cyclic voltammetry, potentiostatic deposits, potential steps and C_E vs. potential curves, it was designed a square wave pulsating overpotential treatment that allows the obtaining of coatings of different chrome species on copper substrate starting from a standard chrome plating bath. Properly adjusting the frequency and lower and upper potential values of the SWPO signal it was possible to obtain cracked and crack free metallic chromium coatings and chromium oxide and hydroxide mixtures films. The oxygen content and surface hardness of these coatings can be controlled as well. Different deposit morphologies were obtained: smooth metallic surfaces, very well facetted crystallites arrangements and leaf type structures. The color of each type of coating also varied from white bright metallic finish for the cracked and crack free metallic coatings, light gray for the facetted crystallites, dark gray for the mixed type coating and matt black for the high hydroxide content leaf type structure. This last type of coating was found to be very similar to the black deposits used for solar energy absorption panels.

Some thermodynamic considerations were made regarding the possible mechanism of coating build up during the SWPO treatment and some insight in deposition mechanism could be done.

6. Acknowledgements

The author thank to the Comisión de Investigaciones Científicas de la Provincia de Buenos Aires (CICPBA) for the financial support to carry out the present research paper.

References

[1] Lausmann, G.A., Surf. Coat. Technol. 1996(86-87): p. 814-820.

[2] Mandich, N.V. and Snyder D.L., Modern Electroplating Fifth Edition, p. 205-248. Schlesinger M. and Paunovic M., Editors, J. Wiley & Sons. (2010).

[3] Newby, K.R., ASM Handbook, Vol. 5, Surface Engineering. 1994, ASM International, p. 177-191

[4] Sargent, G.J., Trans. Am. Electrochem. Soc., 1920. 37.

[5] Wolf G., E. Halwax and Kronberger H., Met. Finish., 2010. 108(1): p. 19-27.

[6] Protsenko V. and Danilov F., Electrochim. Acta, 2009. 54: p. 5666-5672.

[7] Zeng, Z., Wang L., Liang A. and Zhang J., Electrochim. Acta, 2006. 52: p. 1366-1373.

[8] Howarth, J.N. and Pletcher D., J. Appl. Electrochem., 1988. 18: p. 644-652.

[9] Mooney, T., Corrosion: Fundamentals, Testing, and Protection, p. 772–785. ASM International (2003).

[10] Aguilar, M., Barrera E., Palomar-Pardavé M., Huerta L. and Muhl S., J. Non-Cryst. Solids, 2003. 329: p. 31-38.

[11] G. B. Smith, R. C. McPhedran and Derrick G. H., Appl. Phys., A36, 193-204 (1985).

[12] Popov, B.N., White R. E., Slavkov D. and Koneska Z,J. Electrochem. Soc., 1992. 139(1): p. 91-98.

[13] Aguilar-Sanchez, M., Palomar-Pardavé M., Romero-Romo M., Ramírez-Silva M. T., Barrera E. and Scharifker B. R., J. Electroanal. Chem. 2010. 647: p. 128-132.

[14] Pesco, A.M. and Cheh H.Y., Modern Aspects of electrochemistry, p. 251-293. Plenum Press (1989).

[15] Puippe, J.C. and Leaman F., Theory and practice of pulse plating. American Electroplaters and Surface Finishers Society, Publisher (1986), p. 109-117

[16] Chandrasekar, M.S. and Pushpavanam M., Electrochim. Acta, 2008. 53: p. 3313–3322.

[17] Giovanardi, R., Soragni E., Fontanesi C. De Renzi V., Del Pennino U. and Foresti M. L., J. Electroanal. Chem., 2005. 576: p. 243-252.

[18] Baraldi, P., Barani G., Fontanesi C. and Soragni E., Intermetallics, 2000. 8: p. 313-319.

[19] Soragni, E., Fontanesi C., Barani G. and Ganzerli V., J. Appl. Electrochem., 2000. 30: p. 1069-1079.

[20] Vashchenko S. V., Solodkova L. N. and Solov'eva Z. A., Russ. J. Electrochem.; Vol. 36, No. 9, 2000, pp. 947-951.

[21] Baraldi, P., Soragni E., Fontanesi C. and Ganzerli V., J. Alloys Compd. 2001. 317-318 p. 612-618.

[22] Gabe D. R., J. Appl. Electrochem., 1997. 27: p. 908-915.

[23] Saghi Beyragh M.R., Khameneh Asl Sh. and Norouzi S., Surface & Coatings Technology 205 (2010) 2605–2610

[24] Pletcher D. and Lin-Cai J., J. Appl. Electrochem., 1983. 13: p. 235-243.

[25] Dobson S.J. and McCormick M., J. Appl. Electrochem., 1987. 17: p. 303-314.

[26] Saiddington, J.C. and Hoey G.R.,J. Electrochem. Soc., 1970. 117(8): p. 1011-1020.

[27] Jiang, L.C. and Pletcher D., J. Appl. Electrochem., 1983. 13: p. 245-252.

[28] Survilene S., Russ. J. Electrochem. Vol. 34, No. 5, 1998, pp. 506-512.

[29] Ryan, N.E., Met. Finish., 1965(January): p. 46-50.

[30] Ryan, N.E., Met. Finish., 1965(February): p. 73-74.

[31] Rosas, W.R. and Robin A., J. Appl. Electrochem., 2001. 31: p. 531-536.

[32] Fang, J.L., N.J. Wu, and Wang Z.W., J. Appl. Electrochem., 1993. 23: p. 495-499.

[33] Leisner, P., Bech-Nielsen G. and Moller P., J. Appl. Electrochem., 1993. 23: p. 1232-1236.

[34] Hoare, J.P.,J. Electrochem. Soc., 1979. 126.

[35] Pourbaix, M., Atlas of Electrochemical Equilibria (1974).

[36] Bratsch, S.G., J. Phys. Chem. Ref. Data, 1989. 18(1).

[37] Conway, B.E., Theory and Principles of Electrode Processes, New York: The Ronald Press Co. (1965).

[38] Griffin, J.L., Plating, 1966(February): p. 196-203.

Author

W. A. Egli
Electroplating and Corrosion Department,
Centre for Paints and Coatings Development
Scientific Research Commission of Buenos Aires, Province (CICBA), Argentina
Email: anelpire3@cidepint.gov.ar
Phone: 0054/2227-15412879
FAX: 0054/2214-831141

CONTACT:

EUGEN G. LEUZE VERLAG KG
Ralf Schattmaier
Karlstraße 4
88348 Bad Saulgau
Germany

Email: ralf.schattmaier@leuze-verlag.de
Phone: +49 0 7581 4801-12
Fax: +49 0 7581 4801-10